Tensile Force-Dependent Neurite Elicitation via Anti-β1 Integrin Antibody-Coated Magnetic Beads

Joseph N. Fass* and David J. Odde[†]

*Department of Chemical Engineering and Materials Science, and [†]Department of Biomedical Engineering, University of Minnesota, Minneapolis, Minnesota 55455

ABSTRACT   Previous work using glass microneedles to apply calibrated, localized force to neurons showed that tensile force is a sufficient signal for neurite initiation and elongation. However, previous studies did not examine the kinetics or probability of neurite initiation as a function of force or the rate of force application. Here we report the use of a new technique—magnetic bead force application—to systematically investigate the role of force in these phenomena with better ease of use and control over force than glass microneedles. Force-induced neurite initiation from embryonic chick forebrain neurons appeared to be a first-order random process whose rate increased with increasing force, and required the presence of peripheral microtubules. In addition, the probability of initiation was more than twofold lower for neurons exposed to rapid initial force ramps (450 pN/s) than for neurons exposed to slower ramps (1.5 and 11 pN/s). We observed a low force threshold for elongation (15–100 pN), which was not previously detected in chick forebrain neurites elongated by glass microneedles. Finally, neurites subjected to constant force elongated at variable instantaneous rates, and switched abruptly between elongation and retraction, similar to spontaneous, growth-cone-mediated outgrowth and microtubule dynamic instability.

INTRODUCTION

Cells remodel their shape and internal architecture in response to mechanical forces that are either generated internally or transmitted from the external environment. An extreme example of this remodeling is the development of neuronal architecture. For example, filopodia must develop tension internally to develop into neurites (Smith, 1994). Alternatively, neurites have been initiated in vitro by localized application of tensile force via glass microneedles (Bray, 1984; Zheng et al., 1991). Furthermore, neurites are believed to elongate in direct response to force generated either by the advancing growth cone (Bray, 1984; Lamoureux et al., 1989), or by growth of a developing organism (Bray, 1984; Harrison, 1935; Weiss, 1941). These phenomena suggest that we can gain insight into the role of internally generated tension in growth-cone-mediated neurite initiation and elongation by applying an external force to neurons and neurites and observing the resulting behavior.

Several interests motivate these investigations. In addition to the outgrowth of individual neurites, force may play a role in brain tissue morphogenesis (Van Essen, 1997), and is of central importance as a mechanism of nervous system trauma (Smith et al., 1999). Furthermore, recent experiments have shown that elongated bundles of neurites can be induced to form in vitro by using a stepper motor to slowly increase the distance between interconnected neurons at rates of 0.7 μm/min (1 mm/day) (Smith et al., 2001). This method could potentially be exploited to create nerve tissue equivalents, and

an increased understanding of neuronal and neuritic responses to force would aid in such an effort. Finally, it would be desirable to "wire up" small networks of neurons in vitro, via force-mediated neurite initiation and elongation, to gain control over the connectivity of such networks, which would be useful in the study of neural information processing.

To date, only one group has performed force measurements during neurite initiation and elongation by using compliant, calibrated glass microneedles to apply subnanonewton forces to neurons and neurites over durations of minutes to hours (Chada et al., 1997; Lamoureux et al., 1989; Zheng et al., 1991). These studies confirmed, as originally observed by Bray, that neurites could be initiated by force applied via glass microneedles that were coated with any of a variety of adhesion-promoting molecules (Bray, 1984). Neurites required force above a threshold to initiate, and elongated at rates proportional to the level of force above a threshold for elongation. In light of these observations, a three-state model for the behavior of neurites responding to force was proposed: 1), retraction at low force, 2), passive viscoelastic behavior at moderate force, and 3), active growth at high force (see Fig. 1 in Heidemann and Buxbaum, 1990).
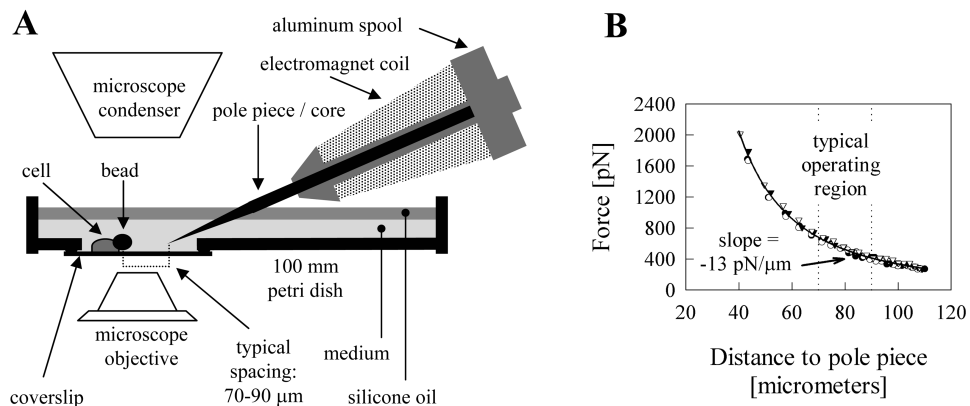
While these results helped to establish tension as an important mediator of neurite initiation and elongation, questions remain. In contrast to chick sensory neurites, no threshold for elongation was observed for forebrain neurites, although it was speculated that this was due to the lower limit of detectability using the glass microneedle technique (Chada et al., 1997). Also, the timecourse of initiation in response to controlled force has not been examined, and there is currently no mechanistic model for neurite initiation in response to applied force. In addition, previous initiation of neurites from chick forebrain neurons with glass microneedles was accomplished via finesse on the part of the operator: force was continuously adjusted to accommodate

A

B

FIGURE 1 Magnetic bead force application. (*A*) Schematic of the experimental setup, with the electromagnet device shown in cross section. The electromagnet was positioned relative to the stage by a micromanipulator, and the motorized stage was positioned manually via joystick or keyboard control. A layer of silicone oil was used to minimize evaporation during experiments. (*B*) Sample calibration curve. A power law curve was fit to data from four independent runs with different beads. Much of the variation in a single run came from taking position difference measurements from a digitized image. Power law curve-fits of different runs deviated from each other by an average of ~2%. The shallow slope of the force-position curve within the typical operating region (e.g., -13 pN/μm at a distance of 80 μm) conferred good control over force, as discussed in Results.

each neuron/neurite to prevent or reverse the development of poor adhesion between cell and needle, or unhealthy thinning of an elongating neurite (S. R. Heidemann, personal communication). While this allowed frequent initiation of robust neurites that could be elongated for several hours, it required a great deal of expertise on the part of the operator, and has been difficult to reproduce. It would thus be desirable to carry out a systematic investigation of neurite initiation and elongation under predetermined force application protocols. Documentation of cellular responses to open loop protocols (i.e., where there is no feedback mechanism to rescue a failing process) would allow better design of closed loop protocols, and thus aid in future optimization, automation, and scale-up of force-induced neuritogenesis for the purposes of creating tissue equivalents. Finally, although microneedles allow the application of force in the nanonewtons-to-hundreds-of-piconewtons range, they are limited in the precision and accuracy with which force can be controlled and measured. Therefore, we wished to reexamine neurite initiation and elongation using a technique that allowed better measurement of and control over force.

Here we report that an emerging technique, magnetic bead force application (MBFA), can be used to apply force with greater accuracy and precision than the microneedle-based technique used previously. In MBFA, a cell surface-attached magnetic bead is subjected to a high gradient magnetic field generated by the sharpened pole piece of an electromagnet. This technique has previously been referred to in the literature as ''magnetic tweezers'' (Bausch et al., 1999), ''single-pole magnetic trapping'' (Huang et al., 2001), ''magnetic manipulation'' (Huang et al., 2002), and ''the magnetic particle method'' (Crick and Hughes, 1949). However, it is important to note that, despite these names, MBFA can only apply force in one direction, and thus cannot by itself determine the position of a manipulated magnetic object. Previously, this technique has been used to measure mechanical properties of cells (Alenghat et al., 2000; Bausch et al., 2001, 1999, 1998; Crick and Hughes, 1949), actin gels

(Schmidt et al., 1996), and lipid vesicles (Heinrich and Waugh, 1996). We used MBFA to apply tensile force to embryonic chick forebrain neurons via 4.5-μm diameter magnetic beads coated with an antibody to β1 integrin, and found that we could initiate and elongate neurites while controlling the applied force to within a few piconewtons. We used this technique to systematically investigate the effects of ultimate force and the rate of the initial ramp to that ultimate force on the frequency and quality of neurite initiation and elongation. Our results both confirm and extend previous findings on the role of cytoskeletal elements in neurite initiation and elongation, and also reveal new features that were obscured by the insensitivity of glass microneedles relative to MBFA. Our experience with both glass microneedles and MBFA indicates that MBFA will facilitate future investigations into force-induced neuritogenesis.

MATERIALS AND METHODS

Magnetic bead preparation

Dynal PanMouse Dynabeads with a diameter of 4.5 μm (Dynal Biotech, Lake Success, NY) were coated with mouse IgG1 anti-chicken β1 integrin (clone W1B10, Sigma, St. Louis, MO) by suspending the beads in 500 μl of 20 μg/ml antibody solution and mixing at 4°C for 2.5 h. Beads were then stored in PBS at pH 7.2 (Gibco, Grand Island, NY) + 0.1% BSA (Sigma) at 4°C, at 10^7 beads per ml. Beads were rinsed several times before and after coating with antibody using PBS + 0.1% BSA.

Cell culture

Cerebral hemispheres were dissected from E7 chick embryos and the meningeal membranes removed. The cerebral tissue was then incubated at 37°C in 0.25% trypsin solution (Gibco) for 15 min, after which the cells were resuspended in medium (F12 supplemented with 5% fetal bovine serum, 5% chicken serum, 100 units/ml penicillin, 100 μg/ml streptomycin, 250 ng amphotericin B/ml, and 20 mM HEPES, adjusted to pH 7.3, all components from Gibco) and dissociated by triturating five times through a 21-gauge syringe needle. One hemisphere in 10 ml of media yielded a suspension density of ~6.8 × 10^5 cells per ml, and cells were plated at a surface density

of 10^5 cells per cm^2 into a 200-μl well, formed by a coverslip glued under a 12-mm hole drilled off-center in the bottom of a 100-mm petri dish. Cells were incubated at 37°C for 30 min, after which 15 ml of serum-free media (similar to above; F12 supplemented with N2, antibiotic/antimycotic, HEPES, all from Gibco) was pipetted into the dish. This relatively large volume was used to minimize changes in ionic strength due to evaporation during incubation on the stage, and to prevent the meniscus around the electromagnet pole piece (see below) from interfering with visualization. After placing the dish on the microscope stage, 20 μl of suspended antibody-coated beads were added directly above the well, and 5 ml of poly-dimethylsiloxane oil (Dimethylpolysiloxane, 5 cSt; Sigma) was added above the medium to reduce evaporation. Experiments were performed on a Zeiss Axiovert 100 inverted microscope (Zeiss, Thornwood, NY) enclosed in a styrofoam enclosure kept at 37°C by a Nevtek ASI 400 Air Stream Incubator (Nevtek, Burnsville, VA). Cells were observed using a Zeiss 40× DIC objective lens (Plan Neofluar, 0.75 NA), Hamamatsu C2400 CCD camera, and Hamamatsu Argus 20 image processor (Hamamatsu, Bridgewater, NJ). Time-lapse video was recorded using a Panasonic AG6740 SVHS recorder (Panasonic, Secaucus, NJ), and still images were captured using an LG3 framegrabber card (Scion, Frederick, MD) and Scion Image software.

Drug treatments

Nocodazole and latrunculin A (Biomol, Plymouth Meeting, PA) were stored at −20°C in DMSO (Sigma). Drug dissolved in media at ~200× final concentration was gently added to culture dishes and mixed by repeated exchange of a small volume of fluid by pipette, which resulted in homogeneous mixing, as verified by simulated mixing using methylene blue dye. The final concentration of DMSO in treated dishes was 0.1%.

Immunocytochemistry

To visualize MTs without interference from soluble tubulin we used a previously established protocol that allows for fixation of polymerized tubulin while allowing for the extraction of tubulin subunits (Black et al., 1996; Gallo and Letourneau, 1998, 1999). Briefly, we simultaneously fixed and extracted cells in warmed cytoskeletal buffer (10 mM MES, 138 mM KCl, 3 mM MgCl$_2$, and 2 mM EGTA, adjusted to pH 6.0; all components from Sigma) containing 0.2% glutaraldehyde and 0.1% Triton X-100 for 15 min by perfusing through a micropipette pulled and broken to a bore size of ~50 μm and positioned next to the target cell. Subsequent steps were carried out at room temperature. Fixed cells were incubated with 1 mg/ml sodium borohydride in Ca^{2+}- and Mg^{2+}-free PBS (15 min), followed by three rinses in PBS (30 min), further permeabilization with 0.5% Triton X-100 (10 min), and an additional three rinses in PBS (10 min each). Next, cultures were blocked by incubation with 0.1% Tween 20 in PBS (10 min), and then incubated with FITC-conjugated mouse anti-tubulin (Sigma) and TRITC-conjugated phalloidin (Molecular Probes, Eugene, OR) (1.5 h), followed by three rinses with 0.1% Tween 20 (30 min), a brief rinse with de-ionized water, and mounting in Clearmount solution (Zymed, San Francisco, CA). Fluorescent images were obtained using a Zeiss 100×, oil-immersion DIC objective (Plan Apochromat, 1.4 NA) and frame-integrated using a Hamamatsu Argus 20 image processor.

Electromagnet construction

Electromagnet devices were constructed by following a previously published design (Bausch et al., 1999, 1998) with minor modifications. Briefly, an electromagnet consisted of a custom-made aluminum spool, which was positioned with a Narishige MHW-3 hydraulic micromanipulator (Narishige International USA, East Meadow, NY) and wrapped with a coil consisting of ~7000 turns of 30-AWG magnet wire (Belden, St. Louis,

MO), and a core extending out from one end of the coil to a sharpened tip (Fig. 1 A). The material of this core/pole piece was electrical iron, a magnetically soft steel alloy. The electrical iron was obtained from scrap in a local shop, and its material and magnetic properties were not assessed. It is likely that any magnetically soft, high-permeability alloy would serve as well, and would probably reduce remanent magnetization of the pole piece. The dimensions of the core were 2-mm in diameter × 135-mm in length, with the last 5 mm sharpened to a fine point that had a radius of curvature of ~20 μm. This point was then flattened on the bottom (the side to be brought near to the coverslip) so that the sharp edge could be manipulated to within 10 μm of the substrate. Approximately 30 mm at the sharpened end protruded from one end of the aluminum spool, which served to support the coil, yet was hollow to accommodate the core/pole piece. The coil covered ~75 mm of axial length along the spool and averaged 10 mm in diameter, tapering toward the end from which the core protruded to facilitate positioning beneath the microscope condenser. The pole piece was coated with a thin coat of toluene and formaldehyde-free nail polish (Wet 'n Wild, North Arlington, NJ) to prevent protein-metal interaction. Without this coating, sending current through the electromagnet in serum-containing media, or even serum-free media with cells, resulted in deposition of an unidentified gel on and around the pole piece (presumably precipitated protein). Constant current was supplied to the electromagnet by a standard 3-Amp DC power supply (Hewlett-Packard, Palo Alto, CA).

Calibration

Electromagnets were calibrated by applying force to 4.5-μm diameter Dynal magnetic beads suspended in 60,000 cSt silicone oil (DMPS-60M, Sigma). 2 μm diameter polystyrene beads (Bangs Laboratories, Fishers, IN) were used as nonmagnetic reference particles to detect and correct for convective drift. Moving averages of positions taken from video recordings of these experiments were used to obtain velocity versus position measurements. Stokes' law ($F = 6\pi\mu Rv$; where F is the force due to friction acting on a particle of radius R traveling at velocity v through a fluid of viscosity μ) was then used to calculate force versus position, and final calibration curves were obtained by fitting pooled data from multiple runs with multiple beads using a power law equation (Fig. 1 B).

Force application

The electromagnet, held by a Narishige hydraulic micromanipulator, was manipulated so that its tip was between 10 and 15 μm above the cell culture surface. In the first set of experiments, after positioning the stage so that a cell-attached bead was just beyond the desired distance (on the order of 80 μm, depending on the desired force), current was manually increased over ~20 s, after which the stage was moved relative to the electromagnet over the next ~20 s, so as to advance the bead closer to the pole piece until the desired location/force was reached. The current followed a sigmoidal increase over time, increasing most rapidly when the voltage was sufficient to supply the current required by a small custom-built current controller. Because force was roughly proportional to current, force was assumed to follow a sigmoidal increase as well. In the next set of experiments, the cell was brought to the desired position first, after which current (and thus force) was increased linearly at a desired rate by means of a voltage signal (from an AT-MIO-16E board controlled by LabView software; National Instruments, Austin, TX) fed to a custom-made current controller. The current levels used were in the range of 0–60 mA. We could not detect any heating of the coil even after hours of use at these current levels. After the ramp-up period, force was clamped at a desired level by manually adjusting the position of a motorized stage (Cell Robotics, Albuquerque, NM) to maintain constant position. Because the angle of force application was ~5–10° above horizontal neither the bead nor the neurite were in contact with the surface after the first few μm of the neurite.

RESULTS

Force application with magnetic beads was simple and robust

We found that MBFA for the purposes of neurite initiation and elongation was relatively simple and technically easier to perform than microneedle-based force application. Construction of the electromagnet was straightforward and inexpensive (see Materials and Methods, and Fig. 1 *A* for setup). In addition, force application was both precise and accurate, as shown by the reproducibility of force measurements during calibration (Fig. 1 *B*, and see below), and by virtue of the single-step calibration (as opposed to calibration of glass microneedles, which requires multiple steps). We performed calibration of the electromagnet as described in Materials and Methods and calculated percent fluctuations ($100\times$ mean $\pm$ SD) between force values. Data from individual runs with a single bead were fit empirically with a power law equation, and the fitted curves were compared to calculate deviations between runs. Force deviations averaged 1.9% between different runs using the same bead (similar to that reported in Bausch et al., 1998), and 2.1% between different beads (compared to 15–20% reported in Bausch et al., 1998). These deviations were calculated for the range of distances used in experiments ($\sim$60–110 μm); deviations outside this range were sometimes larger.

Force clamping during experiments was performed as described in Materials and Methods. Briefly, the position of the bead was held constant with respect to the electromagnet pole piece at distances of $\sim$70–90 μm (Fig. 1), by manually adjusting the position of a motorized stage, as needed (adjustments of 0.25 or 0.5 μm were made as frequently as several times per s, depending on neurite-length changes). As shown in Fig. 1 *B*, this is a region of low slope in the force vs. position curve. Consequently, unintentional deviations in the bead position resulted in small deviations in force. To quantify our level of control over force by this method, we analyzed video from experimental manipulations of beads attached to cells. During experiments, beads experienced root-mean-square deviations in position (from the setpoint) of typically 0.25 μm, which corresponded to deviations in applied force of $\sim$2–4 pN. Although Heidemann and and co-workers did not report in detail on the extent of control over force achieved with glass microneedles, they estimate their typical level of force deviations to be $\sim$50–80 pN (S.R. Heidemann, personal communication). In addition, the "stiffness" (Δforce/Δdisplacement) of the microneedles they used was in the range of 30–70 pN/μm (Chada et al., 1997), compared to the stiffness of the force field in this study of $\sim$12 pN/μm. Thus, assuming equal levels of control over position, our current implementation of MBFA can achieve approximately three- to sixfold better control over force than the glass microneedle technique.

Neurite initiation

Embryonic chick forebrain neurites could be initiated and elongated by force applied via magnetic beads

We used primary cultures of embryonic chick forebrain dissected at E7, which are almost entirely free of glia (Pettmann et al., 1979; Sensenbrenner et al., 1978; Tokioka et al., 1993), and have previously been characterized using glass microneedles (Chada et al., 1997). We applied constant force at seven different levels from 100 to 2000 pN in half-hour-long bouts to 265 chick forebrain neurons using magnetic beads coated with anti-β1 integrin antibody. Of these, 198 bouts began with a 40-s ramp-up period to the desired ultimate force, and an additional 67 were performed using two different initial ramp rates (discussed below). Force application bouts were performed 1.5–10 h after plating the cells. Bead adhesion and neurite initiation was integrin-mediated, as beads coated with irrelevant mouse IgG detached cleanly before the end of 40-s ramps to 330 pN in 10 cases, and in an 11th case within 30 s after the end of the ramp. Force applied to cell-surface-attached beads resulted, in about half the cases, in the initiation and elongation of uniform caliber cytoplasmic processes (Figs. 2, *A* and *B*, and 3 *A*; $N = 128$ out of 265) that contained both actin filaments and microtubules (Fig. 2 *C*). In these cases, force application was continued beyond the first half-hour. In other cases, beads remained attached but did not cause process initiation (Fig. 3 *A*; $N = 68$ out of 265), or else detached cleanly before initiating a process (Fig. 3 *A*; $N = 69$ out of 265). The vast majority of elicited processes formed with their distal tips attached to the beads ($N = 125$), but three processes formed with their tips attached to the substrate as the soma were lifted off the surface by the bead. Beads were never completely engulfed by their cells, and the area of contact appeared to range from the cross sectional area of a neurite ($\sim$1 μm^2) to half the bead surface area ($\sim$30 μm^2). Elicited processes often exhibited active filopodia and vesicle/organelle transport along the shaft, and concentrated filopodial activity at the site of bead attachment. Finally, processes had the ability to adhere to the substrate, after which they exhibited active growth cones. Hence, we refer to these processes as neurites.

The probability of neurite initiation increased rapidly above a threshold force

Fig. 3 *A* shows the fraction of cells that initiated neurites within a half-hour after the initial force ramp-up. Also shown is the fraction of cells that failed to initiate neurites within the first half-hour, and the fraction of cells whose beads detached cleanly without initiating a neurite. The initiation frequency increased rapidly from 100 to 450 pN, and there is a clear optimum at 450 pN in the fraction of cells initiating neurites, due to the overlapping trends in bead detachment and failure to initiate. Initiation rarely occurred after the first half-hour,
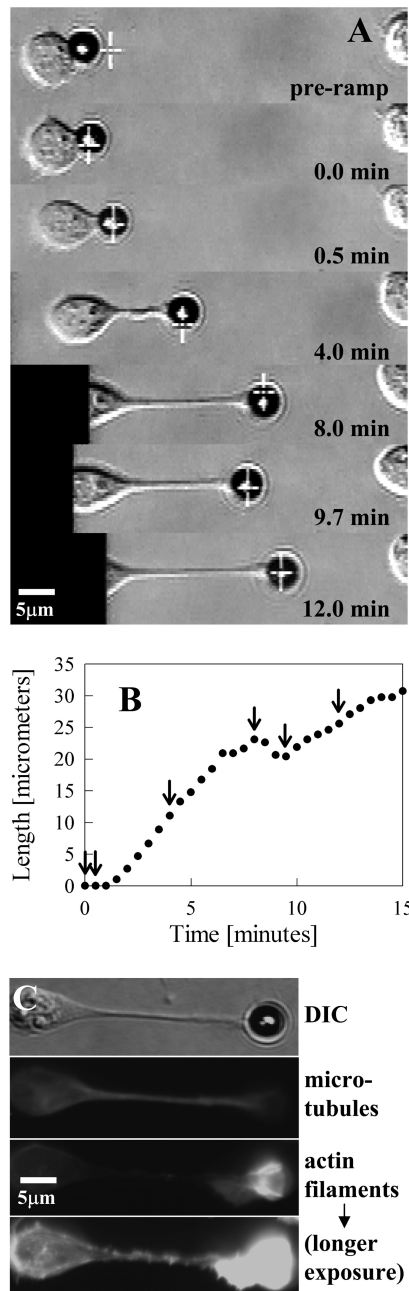
and then only at low force. Fig. 3 B shows the fraction of cells that initiated neurites out of the population of cells whose beads did not detach. A Gaussian cumulative distribution function (the integral of the Gaussian) was fit to this initiation frequency data, as shown in the inset to Fig. 3 B. This distribution, with a mean of 310 pN and a standard deviation of 110 pN, represents the distribution of initiation force thresholds, if it is assumed that at each level of force all neurons with thresholds lower than that level initiate neurites. These values closely match previously reported values, as measured using calibrated glass microneedles (310 ± 220 pN, mean ± SD; Chada et al., 1997).

Neurite initiation times were exponentially distributed and dependent on force

During the ramp-up period, beads moved across cell bodies at widely variable rates, but we found that neurite initiation was not correlated with initial bead position or rate of movement across the cell surface (data not shown). In all cases, beads reached the side of the cell closest to the pole piece during the ramp-up or within the following 30 s. Neurite initiation, which often occurred at some delay after the onset of force application, was similar to previous descriptions (Zheng et al., 1991). Briefly, beads were pulled away from the cell body, often creating a "nubbin" and distending the cell body to a variable extent. Sometimes the process paused at this stage, and the bead was pulled back and forth, although this motion exhibited no obvious oscillation frequency. Initiation was usually accompanied by "necking down"—or simultaneous narrowing and elongation—of the nubbin or attached portion of the cell, so that eventually an even-caliber, elongating process connected the cell to the bead. Often this necking down seemed to result in relaxation of the cell body back away from the bead, allowing it to regain its original shape. Fifty-two percent of the processes initiated before or at the end of the ramp-up period; the rest initiated later in the 30-min bout. As shown in Fig. 4 A, initiation times appeared to be distributed exponentially. In addition, higher forces shifted the distribution of initiation times toward shorter times. Fitting the distributions shown in Fig. 4 A with the equation: $f = 1 - e^{-kt}$ allowed us to calculate the constant k for each force regime. The probability of an exponential fit for each force regime was tested with Monte Carlo simulation (described in the caption for Fig. 4), and the probabilities of exponential fits were determined to be $p = 0.09$ (*low force*), $p = 0.33$ (*medium force*), and $p = 0.8$ (*high force*). Thus we could not reject an exponential fit for any force regime. As shown in Fig. 4 B, k increased monotonically with force.

FIGURE 2 Characterization of elicited neurites. (A) Neurite initiation and elongation in response to applied force (450 pN). Debris on the surface was used as a fiduciary mark to align images so that the surface (and stage) appears to be stationary; in reality the stage was moved so that the separation between the bead and the pole-piece tip (off camera to *right*) remained constant. Elongation of the neurite sometimes required movement of the cell body beyond the edge of the camera's field of view, hence the blacked-out regions (at *left* in images) after 4 min. A cursor (*white crosshairs*) overlaid by the image processor was used to assist in positioning, which was done manually via computer control of a motorized stage. (B) Neurite length history corresponding to sequence in A. In cases where the cell body moved relative to the surface, lengths were measured from the bead to the right edge of the soma where the membrane appeared to taper to an even caliber. Otherwise, length was judged by movement of the bead relative to stationary surface debris. Arrows indicate time points corresponding to the images in A that were taken during force application. (C) Immunocytochemical staining

of a force-initiated process (not the one shown in A) showing the presence of both microtubules and actin filaments in the neurite. As described in Materials and Methods, samples were simultaneously fixed and extracted to reduce background signal from free tubulin subunits.
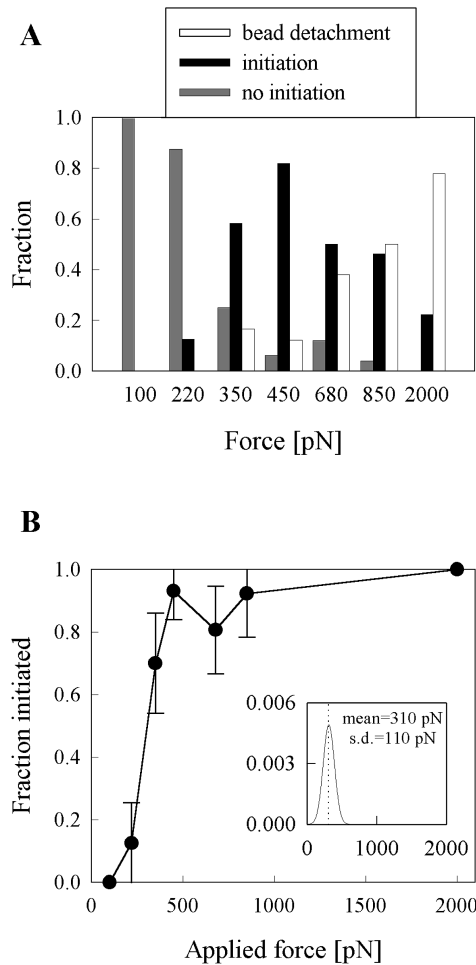
A

B

FIGURE 3 (*A*) Probability of each outcome—neurite initiation, no initiation, and bead detachment—as a function of applied force. All experiments performed with a 40-s initial force ramp are plotted. Sample numbers in each force category are: $N = 11$ (100 pN), 24 (220 pN), 36 (350 pN), 33 (450 pN), 50 (680 pN), 26 (850 pN), and 18 (2000 pN). Note that neurite initiation reaches a maximum at 450 pN, due to increasing failure to initiate toward lower forces and increasing bead detachment toward higher forces. (*B*) The fraction of cells (whose beads remained attached) that initiated neurites in response to applied force during the first half-hour of force application is plotted. Error bars represent the 95% confidence interval calculated assuming a binomial distribution of the number of initiation events. Briefly, given the sample probabilities of initiation (*p*) and no-initiation ($q = 1 - p$) measured from *n* samples, the standard deviation expressed as a fraction of the total number of trials is $(pq/n)^{0.5}$ and the 95% confidence limits are 1.96 × the standard deviation. (*Inset*) Initiation frequency data were fit with a Gaussian cumulative distribution function (the integral of a Gaussian), and the inset shows the corresponding Gaussian (*x*-axis is force in pN; *y*-axis is density in pN^{-1}), which represents the distribution of initiation thresholds. The mean of the probability density function was 310 pN, and the standard deviation was 110 pN. This analysis assumes that at each level of force, all cells with thresholds below that level initiate neurites. Thus, the frequency of initiation at a particular force *F*, as shown in the main graph, would be determined by the integral of the curve shown in the inset from 0 to *F*.

Neurites were less likely to initiate when the initial ramp rate was high

Because we originally kept the duration of the force ramp
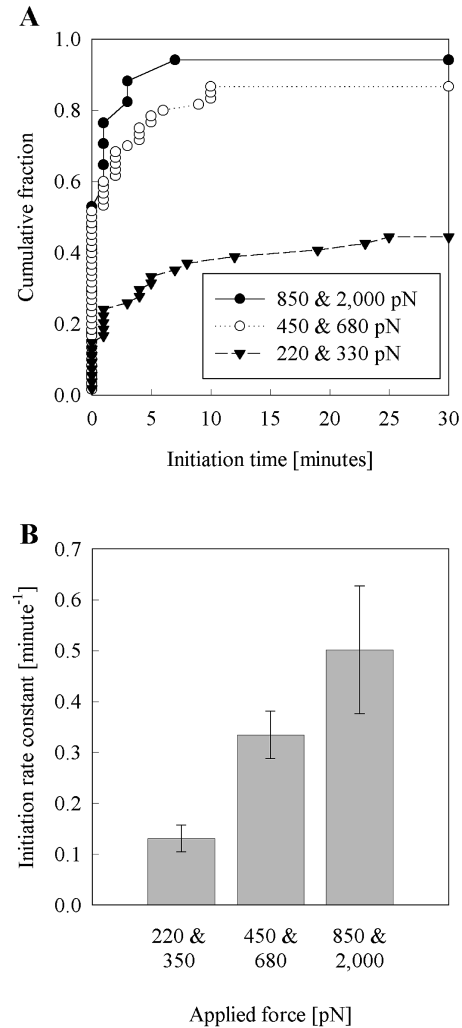
A

B

Applied force [pN]

FIGURE 4 Distribution of initiation times and its dependence on applied force. (*A*) Cumulative distributions of initiation times are shown for low (220 and 330 pN), medium (450 and 680 pN), and high force (850 and 2000 pN). The mean initiation times at medium and high force are not significantly different by *t*-test ($p = 0.36$), but are significantly different between low and medium ($p = 0.041$) and low and high force ($p = 0.020$). (*B*) Constants *k*, from exponential curves of the form: $f = 1 - e^{-kt}$ fit to the distributions in *A*, increased with increasing force. The probability of an exponential fit for each force regime was tested with Monte Carlo simulation, as follows: simulated data sets of the same size as the experimental sets were generated by using random numbers to generate exponentially distributed initiation times, using the value of *k* fit to data from each force regime. These simulated times were used to generate a cumulative distribution, and the sum of squared error (SSE) between this distribution and the best fit exponential. This process was repeated 1000 times, and the SSE of the experimental data (relative to the same fitted exponential) was ranked among the simulated SSE's to obtain a *p*-value (i.e., if the SSE of the experimental data ranked the 100th largest out of 1000 simulated SSE's, then its *p*-value would be $100/1000 = 0.1$). The probabilities of exponential fits were determined to be $p = 0.09$ (low force), $p = 0.33$ (medium force), and $p = 0.8$ (high force).

constant at 40 s for all ultimate forces, the rate of this ramp increased from 2.5 pN/s (at 100-pN ultimate force) to 50 pN/s (at 2000 pN ultimate force). To test the dependence of the outcome distribution on the ramp rate alone, we performed

additional experiments at an ultimate force of 450 pN using initial ramp rates of 1.5 and 450 pN/s (compared to 11 pN/s from the original data set), corresponding to 5 min and 1-s ramp durations, respectively. Between experiments at the two lower rates (1.5 and 11 pN/s) there were no significant differences in behavior in terms of the frequencies of bead detachment, neurite initiation, and failure to initiate, as shown in Fig. 5. However, for experiments using the highest ramp rate (450 pN/s), each outcome's observed frequency was significantly different than for experiments using 11 pN/s ramps. The frequency of bead detachment increased from 0.12 to 0.32, the frequency of initiation decreased from 0.82 to 0.32, and the frequency of failure to initiate increased from 0.06 to 0.35, concurrent with a 40-fold increase in the ramp rate (11–450 pN/s). In contrast, in the original, constant ramp-time experiments, the frequency of neurite initiation increased from zero to one (Fig. 3 B), concurrent with the 25-fold increase in ramp rate (2.5–50 pN/s), due to holding the duration of the ramp constant at 40 s over the range of ultimate forces (100–2000 pN). Therefore, the increase in neurite initiation frequency shown in Fig. 4 was in response to the increasing ultimate force, and not the increasing ramp rate.

The cytoskeletal drugs latrunculin A and nocodazole interfered with normal initiation and elongation

To assess the importance of actin filaments and microtubules in force-induced neurite initiation, we used latrunculin A and nocodazole pretreatments before force-clamp experiments. Exposure to 1 μM latrunculin A for 15 min completely abolished phalloidin staining for F-actin in most cells, but did not appear to affect the microtubule distribution or intensity, as assessed by immunocytochemistry. Exposure to 6.6 μM nocodazole for 1 h largely depleted microtubules in the short processes sprouted by chick forebrain neurons soon after plating, but did not appear to affect F-actin distribution or intensity (data not shown). After exposure to drug, we applied force to cell-attached beads using a 40-s ramp-up to 450 pN, and outcomes were recorded as shown in Fig. 6. Both drugs significantly increased the frequency of bead detachment, and prevented the formation of robust neurites. Instead, all processes initiated under drug treatment elongated at very high rates (>250 μm/min) and thinned and
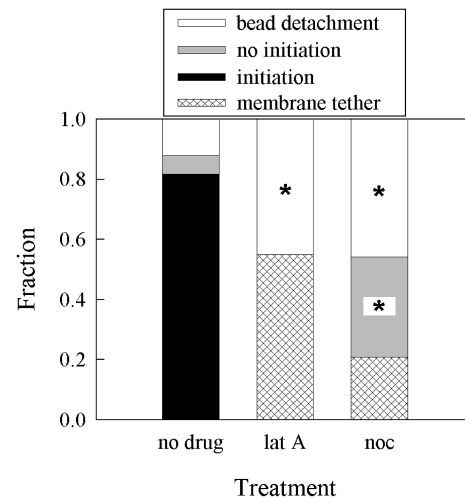
FIGURE 6 Probability of bead detachment, no initiation, process initiation, and membrane tether formation after treatment with cytoskeletal drugs. Pretreatment with 1 μM latrunculin A for 15 min completely abolished F-actin in most cells. Pretreatment with 6.6 μM nocodazole for 1 h reduced microtubule immunofluorescence dramatically in minor processes, but not in cell bodies. The initial ramp rate was 11.2 pN/s, and the ultimate force was 450 pN for all treatments. Sample sizes in each category were $N =$ 33 (no drug), 20 (lat A), and 24 (noc). Both latrunculin A and nocodazole significantly increased the frequency of bead detachment (*, $p < 0.01$ as tested by Monte Carlo simulation, described in the caption for Fig. 5). Latrunculin-A-treated cells initiated membrane tethers 55% of the time, and nocodazole treated cells initiated tethers 21% of the time, whereas no membrane tethers were initiated from control cells. Tethers were very thin and uniform in appearance, elongated faster than 250 μm/min, and broke less than 15 s after initiation. In contrast, all processes initiated from control cells elongated slower than 50 μm/min (most elongated at ~0.5–5.0 μm/min), and only five out of 26 thinned and broke less than 1 min after initiation. Finally, nocodazole-treated cells retained their attached beads but failed to initiate a process 33% of the time (no-initiation category), compared to 6% of the time for untreated cells.
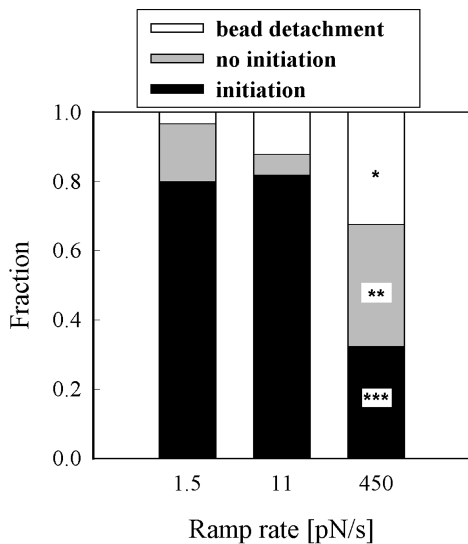

FIGURE 5 The probabilities of neurite initiation, no initiation, and bead detachment are shown as a function of the initial force ramp rate; ultimate force was 450 pN for all ramp rates. Sample sizes in each category were $N =$ 30 (1.5 pN/s), 33 (11 pN/s), and 37 (450 pN/s). The probabilities of each outcome were not significantly different between the two lower ramp rates, but each was significantly different at 450 pN/s than at the two lower ramp rates (*, $p < 0.03$; **, $p < 0.005$; ***, and $p < 0.001$) as tested by Monte Carlo simulation. Briefly, expected outcome frequencies were calculated by lumping the "control" and "test" data together. Then, two groups of the same size as the original data sets were generated by comparing random numbers to these expected frequencies to simulate outcomes. The simulation of the experiment was repeated 1000 times, and the absolute differences in observed outcome frequencies were ranked among the absolute differences obtained from the simulated data sets to obtain a p-value for each category.

broke within 15 s after initiation, suggesting that they were membrane tethers largely devoid of cytoskeleton. In addition, cells treated with nocodazole failed to initiate a process in response to 30 min of constant force application more frequently than untreated cells (0.33 for nocodazole-treated cells versus 0.06 for untreated cells; Fig. 6).

Neurite elongation

After initiation, neurites were held at constant force at the same level as that used to initiate them. Time-lapse video recordings of all elicited neurites were analyzed to acquire neurite length histories, shown for each force in Fig. 7. In most cases the cell bodies remained stationary throughout the period of elongation, and length was measured by tracking the position of the bead's center relative to debris on the coverslip. However, in some cases the cell body was seen to migrate during the bout, and neurite length was measured by taking the distance from the left edge of the bead to the end of the tapered portion of the process proximal to the cell body. Although some neurites appeared to elongate at variable average rates (e.g., the three histories ending at ~30, 40, and 50 min and ~25, 15, and 25 μm, respectively, in the 450 pN panel), most length histories appear roughly linear, with varying degrees of fluctuation in growth rate on short timescales (min).
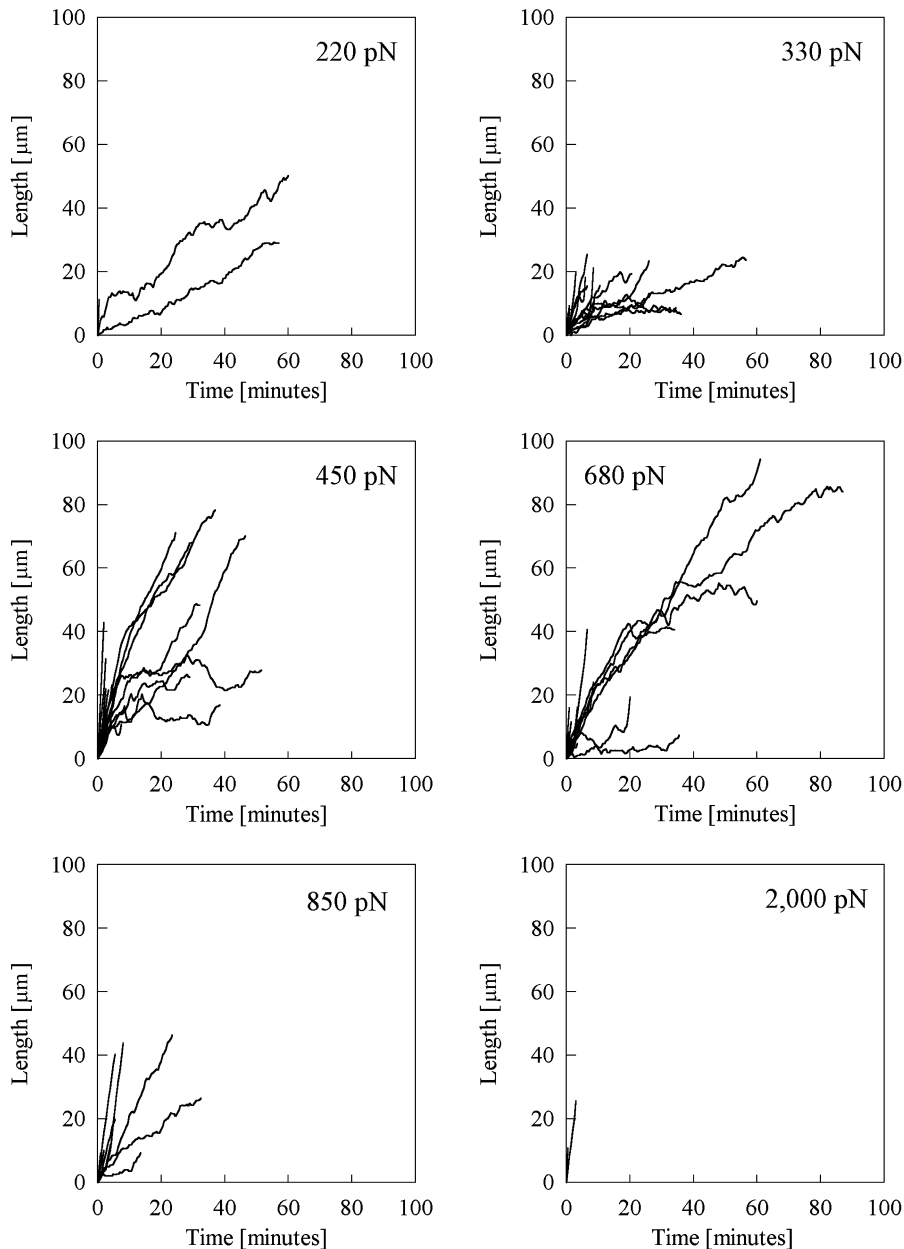

FIGURE 7 Neurite-length histories for all experiments with constant ramp-time. Length histories were constructed by taking length measurements at 30-s intervals from time-lapse video recordings. Duplicate measurements by the same or a different person had RMS deviations of typically 0.26 μm. These length histories illustrate several features discussed in the text: variability in average and short-term elongation rate, and spontaneous reversals. Experiments in which ramp time was varied are not shown, but length histories from these experiments exhibited similar features.

Not all neurites supported sustained growth

Visible in the neurite length histories shown in Fig. 7 are many curves that terminate after only a few minutes. Length history measurements were terminated at early times either when the bead was suspected to be in contact with another cell or when the neurite thinned out and broke, releasing the bead. Some neurites elongated rapidly from the moment of initiation, and soon thinned and broke, sometimes in the first 30 s after initiation. However, unlike the membrane-tether-like processes initiated from drug-treated cells, many of the processes initiated from untreated cells that thinned and broke persisted for several minutes, and all elongated at average rates <50 μm/min. In addition, after thinning and breaking, these processes retracted by kinking and curling up in a nonuniform way until they were either absorbed into the cell body or fell to the coverslip surface, at which time they often exhibited filopodial or lamellipodial activity. Although it was difficult to measure the rate of retraction, we estimated a maximum rate of 60 μm/min for the most distal segment of the processes that had been proximal to the bead. Subsequent retraction of even the thinnest processes occurred more slowly than this maximum rate. In contrast, previous studies report that membrane tethers elicited from neuronal growth cones are formed at much lower forces ($\sim$10 pN), are highly sensitive to force (elongating at $\sim$500 μm/min at 15 pN), and at zero force they retract completely at $\sim$600 μm/min while curving in a smooth, serpentine fashion (Dai and Sheetz, 1995; Hochmuth et al., 1996). Finally, we fixed and stained a process that was elongating rapidly ($\sim$6 μm/min) and appeared to be headed for a thin-and-break event, and it contained both actin filaments and microtubules (data not shown). Given this evidence we feel confident that even these short-lived, rapidly elongating processes were not membrane tethers.

Previously, thinning and breaking behavior was infrequently observed in elicited chick sensory neurites, although when poisoned with nanomolar concentrations of vinblastine, thinning and breaking was observed in about two-thirds of these neurites (Zheng et al., 1993). However, thinning and breaking behavior was not reported for chick forebrain neurites (Chada et al., 1997). In contrast, $\sim$62% of the neurites elicited in the present study thinned and broke in less than 10 min (many of these length histories are obscured, near the origin, in the graphs shown in Fig. 7). Thinning and breaking occurred either in neurites that elongated rapidly over their whole history (as described above) or in slowly elongating neurites after a dramatic increase in elongation rate (from $\sim$1 μm/min up to 5–20 μm/min) that was usually concurrent with thinning of the neurite proximal to the bead. In contrast, bead detachment during the initial ramp-up period was almost instantaneous and usually occurred without visible deformation of the cell body. Therefore, we suspect that while initial bead detachment is due to all-at-once failure of the bead-integrin

and/or integrin-cytoskeleton linkages, thinning and breaking events occur in neurites in which the cytoskeletal matrix is unable to support the applied force, and successive failure of bonds between cytoskeletal elements leads to increasing tensile stress (force-per-filament-cross-sectional area) and rapid elongation that would outstrip any reinforcement of the cytoskeleton, inevitably leading to failure. In support of this hypothesis, we observed that many of the neurites that failed in this way underwent rapid, jerky elongation events in the seconds before bead detachment. In addition, all neurites that were elongating faster than an average of 3.3 μm/min thinned and broke in less than 10 min (whereas only $\sim$38% of the neurites that elongated at an average rate slower than 3.3 μm/min thinned and broke), and neurites were more likely to thin and break sooner if they were elongating faster (data not shown).

On long timescales, neurites elongated at all applied forces above 15 pN at rates that are consistent with previously reported values

We chose not to analyze the length histories of neurites that thinned and broke earlier than 10 min, out of concern that their structure was different from that of more robust neurites. Length histories from 29 neurites (out of 94 total) from the original 40-s-ramp-up experiments that persisted longer than 10 min were analyzed further. As shown in Fig. 8, each of these neurites underwent net growth after initiation during the time they were observed, at average rates similar to those
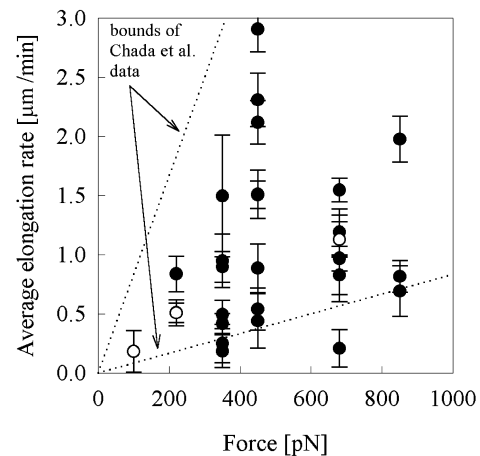

FIGURE 8 Average elongation rates of robust neurites as a function of force (*solid circles*; 26 neurites). Also plotted (*unfilled circles*) are three rates from neurites that initiated after 30 min from the onset of force application. Error bars are mean $\pm$ SE, calculated from the distribution of instantaneous rates taken at 30-s intervals for each neurite. Previously reported rates for force-induced chick forebrain neurite elongation (Chada et al., 1997) fall in the region between the dotted lines. Note that Chada and co-workers did not observe a minimum force for elongation (hence the zero intercept of the lines), whereas we observed retraction of all neurites tested at 15 pN (data not shown).

observed previously for chick forebrain neurites (Chada et al., 1997). Observation was usually terminated after ~1 h unless the neurite thinned and broke or the bead contacted another cell. For the 29 robust neurites, these observation times ranged from 10.5 to 87.0 min with a mean of 38 min. Average elongation rates ranged from 0.18 to 2.9 μm/min, with a mean of 0.98 μm/min and a standard deviation of 0.68 μm/min. The broad distribution of force sensitivities (elongation rate versus applied force) previously reported by Chada et al. (1997) predicts broadly distributed average elongation rates if rates are measured at a single force for each neurite, as we have done. Thus, our results are not inconsistent with previous observations of a linear correlation between elongation rate and force within individual neurites (Chada et al., 1997; Dennerll et al., 1989; Zheng et al., 1991).

When possible, the current in the electromagnet coil was reduced to zero at the end of the experiment so that the bead and induced neurite would only experience force due to the remanent magnetization of the pole piece. This remanent force was, for one pole piece, measured accurately to be 15 ± 2 pN, after a technique using nonmagnetic reference beads during calibration runs was developed. Due to close agreement with previous, less accurate measurements of the remanent force for other pole pieces (within 10 or 15 pN), we believe that this value was always in the range of 10–30 pN. We exposed six of the 29 robust neurites to this force and observed significant, persistent retraction in all of them. Retraction occurred at a mean rate of 6.8 μm/min over a mean observation time of 5.4 min, and persisted until the neurite had disappeared into the cell body or the remaining neurite was well spread and firmly adhered to the substrate. Previously, chick forebrain neurite elongation was reported to occur at all measurable applied forces. However, the authors reported in that study that they could not confidently apply forces below 100 pN (Chada et al., 1997). Our results show that there is a threshold for neurite elongation of chick forebrain neurites between ~15 and 100 pN.

On short timescales, neurites switched between elongation and retraction, and exhibited normally distributed short-term elongation rates

As shown in Figs. 2 *B* and 7, neurites exhibited a wide range of short-term elongation rates. Many neurites switched back and forth between states of elongation and retraction, despite constant force application, and retraction events sometimes persisted for several minutes. This behavior is shown for one of the 29 robust neurites in Fig. 9, *A* and *B*. In addition, the cumulative distribution of elongation rates (measured at 30-s intervals) for the same neurite is shown in Fig. 9 *C*, indicating a normal distribution. The distributions of the other 28 robust neurites appeared similar to the one shown.
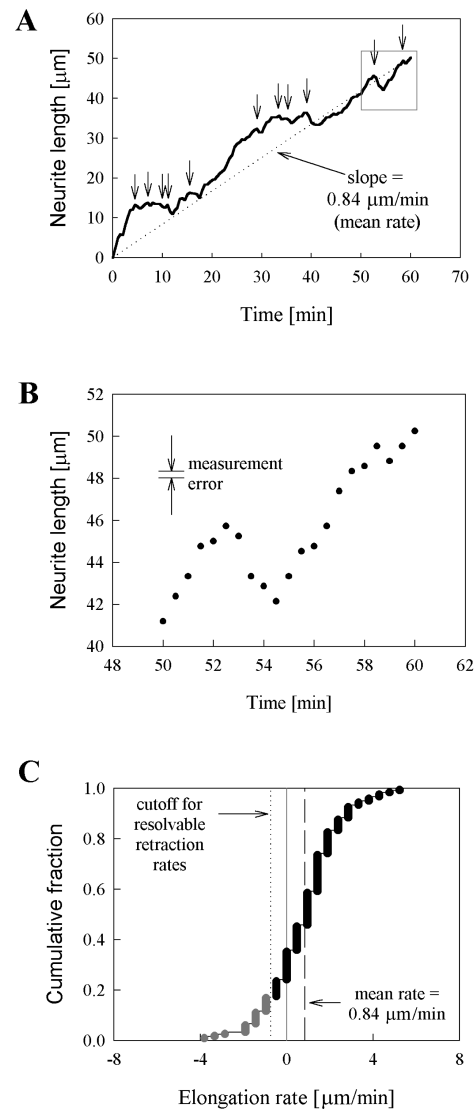

FIGURE 9 Characterization of short-term neurite elongation rate variability. (*A*) A single length history (of a neurite initiated and elongated at 220 pN) is shown, with all resolvable retractions indicated by arrows. We considered a negative length change (occurring over one or more 30-s interval) to be a retraction if its value was >0.37 μm (the expected RMS error for a difference measurement between two consecutive lengths, each with an RMS error of 0.26 μm). The mean elongation rate was calculated from the final length and time (equivalently, the slope of the line through the origin and the final point). (*B*) The region of interest indicated by the box in *A* is shown, enlarged, along with an indicator of the RMS measurement error (0.26 μm). (*C*) Rates of length change were calculated from the 30-s interval length data used in *A*, to calculate the cumulative distribution of instantaneous rates. The cumulative distributions of each of the 29 robust neurites were individually similar in appearance to the distribution plotted in *C*. Also indicated are the cutoff value for resolvable retractions (i.e., rates <0.37/0.5 μm/min = 0.74 μm/min) and the mean elongation rate for this neurite.

DISCUSSION

To investigate the response of neurons to long-term application of tensile force we adapted a relatively new tech-

nique in which magnetic beads were used to apply force to cells via β1-integrins. We intentionally applied force in an open-loop manner where force profiles were predetermined and were applied to cells regardless of outcome, so as to investigate the determinants of both success and failure of neurite initiation and elongation. This paradigm should facilitate future efforts to design closed-loop protocols that will enhance the likelihood of successful initiation and elongation of healthy neurites. Furthermore, an understanding of neuronal responses to defined, well-controlled force stimuli will aid in the formulation of better mechanistic models of neurite initiation and elongation. Our results confirm previous observations that neurites can be initiated and elongated by localized application of tensile force, that in some cases these neurites resemble spontaneously formed neurites in all aspects examined, and that there is a threshold force required to initiate neurites (310 pN). In addition, we went beyond previous analyses to find that lag times between force application and neurite initiation are exponentially distributed, that higher forces result in shorter time lags, and that initiation was prevented by depletion of peripheral microtubules with nocodazole. We also found that neurons that are subjected to higher-rate initial force ramps are less likely to initiate a neurite in response to subsequent application of constant force. Finally, we found that elongating chick forebrain neurites 1), have a previously undetected threshold force (in the range of 15–100 pN) below which they retract; 2), spontaneously switch between elongation and retraction even at constant applied force; and 3), have short-term rates of length change that are normally distributed. Some of these observations were specifically enabled by the use of the MBFA technique, so we first discuss the advantageous features of the technique itself.

The MBFA technique

In our hands, MBFA provided a simple, robust, precise, and accurate means of applying localized force to neurons for the purpose of inducing neurite initiation and elongation. While force can only be applied in one direction with this technique, the range of forces that can be applied is large. The present study and previous reports demonstrate the feasibility of applying forces from several piconewtons (Heinrich and Waugh, 1996) to several nanonewtons (Bausch et al., 2001, 1999, 1998), and the bounds of this range have not yet been fully tested. This range makes the technique attractive in some respects compared to laser trapping or microneedle-based force application. Laser traps have been used to apply forces up to ~100 pN, but concerns about radiation damage to cells and biomolecules make laser trapping a poor choice for manipulations that may last hours (Bustamante et al., 2000). Although glass microneedles have been used to apply tensile forces to neurons and neurites, the microneedles used in previous studies were not accurate <100 pN (Chada et al., 1997). Nevertheless, glass microneedles have been used to

measure forces on the order of 10 pN over timescales on the order of milliseconds (Kitamura et al., 1999). In our experience, this apparent discrepancy is explained by the fact that as microneedle bending compliance is increased to gain better force sensitivity, the resulting microneedles become more sensitive to drift and vibration on various timescales. The MBFA technique, on the other hand, is not subject to these competing constraints. We found that a heavy electromagnet was easier to keep stably positioned than a glass microneedle, and was less susceptible to vibration. In summary, cellular processes involve force levels from nanonewtons down to piconewtons, so it is useful to have a single force application technique that can address this full range with piconewton resolution.

Neurite initiation

Using MBFA, we found that tension applied via magnetic beads was able to initiate and elongate cytoplasmic processes which appeared to be normal neurites. Specifically, the processes exhibited normal neurite morphology at both the light microscopic and immunocytochemical levels, and behaved normally in time-lapse video recordings. Neurite initiation and elongation always occurred along the axis of force application, consistent with the idea that direct transmission of force through the membrane provides a directional cue for outgrowth (Suter and Forscher, 1998).

In addition, we observed that the probability of initiation increased dramatically over the range of 220–450 pN, revealing a threshold force for initiation of 310 ± 110 pN (mean ± SD; Fig. 3). This threshold is essentially the same as reported previously for chick forebrain neurons (310 ± 220 pN, mean ± SD; Chada et al., 1997). Such close agreement indicates the robustness of the initiation process, as it was observed despite the use of different methods of force application, slightly different culture methods, and different bead/needle coatings. Indeed, the fact that neurites have been elicited by artificial force application using surfaces treated with collagen and polylysine (Bray, 1984), collagen and laminin (Lamoureux et al., 1989), concanavalin A (Chada et al., 1997), and now anti-β1 integrin antibody (present study), further confirms that tensile force, rather than a specific cell-surface-molecule-mediated signaling pathway, is sufficient to initiate neurite outgrowth. An intact actin cytoskeleton was required to transmit this force, as cells treated with latrunculin A always released their beads or initiated membrane tether-like processes (Fig. 6). Nocodazole-treated cells also exhibited bead detachment more frequently than untreated cells (Fig. 6), possibly due to disruption of mechanical coupling between microtubules and F-actin (Waterman-Storer and Salmon, 1997).

Intriguingly, we observed an exponential distribution of time lags between the onset of force application and initiation. One potential explanation for this distribution is that cells are individually biased to initiate after different time lags, and

these lags are exponentially distributed. However, cellular characteristics are often normally distributed, and a mechanism that would give rise to individually predetermined initiation time lags that are exponentially distributed across a population is not obvious.

Alternatively, the distribution we observed is consistent with a model of initiation as a first-order random process, with a rate that increases with increasing applied force. Note that this process may involve many steps, but the rate constant for one step must be significantly smaller than the rest for the process to exhibit first-order kinetics, thus giving rise to an exponential distribution of time lags. What is this single random event, or rate-limiting step? When nocodazole was used to depolymerize microtubules in the cell periphery, we observed a significant increase of failures to initiate compared to untreated cells (see Fig. 6 *A*). In other words, even with an intact actin cytoskeleton that could sustain and transfer a force of 450 pN to the interior of the cell, the depletion of peripheral microtubules prevented neurite initiation from taking place.

Our results raise the possibility that tensile stress above a threshold activates the local intracellular environment in the vicinity of integrin binding so as to be receptive to triggering of the initiation process by the arrival of a microtubule plus end. In support of this hypothesis, localized buildup of actin filaments can redirect microtubules in growth cones or developing collateral branches (Dent et al., 1999; Dent and Kalil, 2001; Gallo and Letourneau, 1998; Zhou et al., 2002), and tensile stress can induce microtubule polymerization in non-neuronal cells (Kaverina et al., 2002). Whether by motor-based transport (possibly facilitated by F-actin) or dynamic instability, the exploration of the local environment by a microtubule plus end is equivalent to a random walk on minute timescales, thus the time required for a microtubule plus end to arrive in a nearby activated region would be exponentially distributed. Higher forces would be expected to activate larger regions of the actin cortex, thereby reducing the time required for microtubule arrival. There is further support for this hypothesis from direct observations of spontaneous neurite initiation. Embryonic chick sympathetic neurons have been observed to initiate neurites in vitro after filopodial contact with a bead or cell. A filopodium that made contact would then straighten (indicating tension generation), after which cytoplasm at its base would begin to move anterogradely up the filopodial shaft, but in a saltatory fashion, alternating between advance and retraction (Smith, 1994). Taken together with our results, these observations support the idea that neurite initiation is triggered by the stochastic arrival of a microtubule plus end, which could potentially locally influence cytoskeletal rearrangement via microtubule plus end-associated proteins (Wittmann and Waterman-Storer, 2001).

Another issue that has not previously been examined is that of the rate of force application and its effect on neurite initiation. By ramping up to the same ultimate force at different rates, we found that the fraction of beads that detached during or immediately after the ramp was roughly triple that at the two lower rates (Fig. 5). We suspect that the fast ramps simply selected out the population of beads that were initially poorly adhered to the cell surface. In support of this, there is accumulating evidence that strengthening of cytoskeletal-ECM adhesions in response to applied force occurs over a timecourse of 10s of seconds (Choquet et al., 1997; Riveline et al., 2001) or minutes (Glogauer et al., 1997). Thus, we propose that in our study the slower ramp rates allowed time for reinforcement of initially poor adhesions to take place. More surprising, however, is our observation that the neurons that retained beads after the fast ramps were less likely to initiate neurites (Fig. 5). Although we cannot rule out the possibility that this was due to cell damage caused by the faster ramps, an alternative explanation is that neurons, and cells in general, are sensitive to the rate of change in applied force. Fast force ramps may elicit a mechanoprotective response (Glogauer et al., 1998, 1997; Ko and McCulloch, 2000), effectively raising the threshold force required for initiation.

Neurite elongation

We observed a high rate of neurite thinning and breaking compared to previous results. However, given the similarity of culture systems, and of other measured characteristics (initiation threshold, average elongation rates, etc.), we suspect that the difference is a result of our intentional use of an open-loop method of force application. Future experiments could incorporate feedback control to limit rates of movement during initiation or elongation, and potentially eliminate thinning and breaking. However, an improved understanding of the underlying mechanisms is necessary to further guide the design of automated closed-loop protocols.

Previous workers observed a threshold force for elongation of PC12 and chick sensory neurites (Zheng et al., 1991), but not of chick forebrain neurites (Chada et al., 1997). We were able to apply low force to previously elicited neurites: ~15 pN, which was lower than the force that could confidently be applied with glass microneedles (100 pN, Chada et al., 1997), allowing us to detect a threshold for elongation between 15 and 100 pN; i.e., elongation in all cases at 100 pN or higher, and retraction in all cases at ~15 pN applied force. This observation, enabled by the improved sensitivity of the MBFA technique relative to glass microneedles, confirms the qualitative similarity of chick forebrain neurite behavior to that of other neurites.

A striking feature of the neurite length histories we recorded is the variability in instantaneous elongation rates. At the extreme, this variability resulted in periods of retraction in many neurites, at all forces except 2000 pN. Previously, this degree of variability in force-induced elongation rates has not explicitly been reported, and rate variability is visible only to a small degree in published data (see Fig. 1 in

Zheng et al., 1991). Thus, it was surprising to us that, with better control over force, we still saw a large degree of variability in neurite growth rates. We propose that this variability is an intrinsic feature of neurite elongation. In support of this hypothesis, it has been previously noted that spontaneous switching between growth and retraction occurs both in normal growth-cone-mediated neurite outgrowth (e.g., Katz et al., 1984; Odde et al., 1996), and in cytoplasmic movements in filopodia that are developing into neurites (Smith, 1994).

What is the source of this variability? As a result of their experiments, Heidemann and Buxbaum described neurite behavior in response to applied tensile force with a three-state model: low force causes retraction, moderate force causes passive viscoelastic responses, high force causes active growth, and each force regime is separated by a threshold (Heidemann and Buxbaum, 1990). This model is inherently deterministic as stated, and cannot account for the variability we observed. As an alternative, we first hypothesized that random variation of the diameters of our neurites over time was changing the tensile stress (force per cross-sectional area of a load-bearing element), even as we held force constant. However, we found no correlation between neurite diameter and rate within or between different bouts, although we concluded this based on qualitative observation (quantitation was very difficult because the neurites did not lie in a single focal plane). Nevertheless, it is possible that the number or architecture of load-bearing cytoskeletal elements—presumably actin filaments and/or microtubules—was changing without affecting the appearance of the neurites.

Alternatively, the neurite length fluctuations could be a result of the intrinsic stochasticity of cytoskeletal assembly/disassembly or transport. Heidemann and Buxbaum proposed that applied tensile force could bias the thermodynamics of tubulin subunit addition and thus lead to an increased microtubule assembly rate over long timescales (hours) (Buxbaum and Heidemann, 1992). Over shorter timescales, microtubules could drive the spontaneous switching between neurite elongation and retraction. In support of the role of microtubule assembly dynamics in the observed fluctuations, time-series analyses of both simulated microtubule assembly via dynamic instability and experimentally observed growth-cone advance revealed that the two processes are nearly identical in terms of their power spectra and autocorrelation functions (Odde and Buettner, 1995). Alternatively, there is strong evidence that microtubules are supplied to the ends of elongating neurites via stochastic transport of microtubule fragments by motor proteins (Ahmad et al., 2000; Baas, 2002; Baas and Ahmad, 2001). In either case, fluorescence imaging of microtubules protruding from the neurite shaft into the growth cone revealed significant cross-correlation between growth-cone movements and the advance and retreat of the microtubule front over timescales up to 2 min (Odde et al., 1996). Finally, in the present study, motility of the growth cone was pre-sumably unable to effect neurite length changes by virtue of its attachment to the bead, yet we still observed a normal distribution of displacements, including retractions, similar to previous analyses of growth-cone-mediated outgrowth (Fig. 9; Katz et al., 1984; Odde et al., 1996). Taken together, these observations suggest that stochastic microtubule assembly and/or transport in the neurite shaft or at the base of the growth cone—independent of movement of the growth cone over substrate—are plausible mechanisms giving rise to variability in neurite elongation rate at constant applied force.

REFERENCES

Ahmad, F. J., J. Hughey, T. Wittmann, A. Hyman, M. Greaser, and P. W. Baas. 2000. Motor proteins regulate force interactions between microtubules and microfilaments in the axon. *Nat. Cell Biol.* 2:276–280.

Alenghat, F. J., B. Fabry, K. Y. Tsai, W. H. Goldmann, D. E. Ingber. 2000. Analysis of cell mechanics in single vinculin-deficient cells using a magnetic tweezer. *Biochem. Res. Commun.* 277:93–99.

Baas, P. W. 2002. Microtubule transport in the axon. *Int. Rev. Cytol.* 212:41–62.

Baas, P. W., and F. J. Ahmad. 2001. Force generation by cytoskeletal motor proteins as a regulator of axonal elongation and retraction. *Trends Cell Biol.* 11:244–249.

Bausch, A. R., U. Hellerer, M. Essler, M. Aepfelbacher, and E. Sackmann. 2001. Rapid stiffening of integrin receptor-actin linkages in endothelial cells stimulated with thrombin: a magnetic bead microrheology study. *Biophys. J.* 80:2649–2657.

Bausch, A. R., W. Möller, and E. Sackmann. 1999. Measurement of local viscoelasticity and forces in living cells by magnetic tweezers. *Biophys. J.* 76:573–579.

Bausch, A. R., F. Ziemann, A. A. Boulbitch, K. Jacobson, and E. Sackmann. 1998. Local measurements of viscoelastic parameters of adherent cell surfaces by magnetic bead microrheometry. *Biophys. J.* 75:2038–2049.

Black, M. M., T. Slaughter, S. Moshiach, M. Obrocka, and I. Fischer. 1996. Tau is enriched on dynamic microtubules in the distal region of growing axons. *J. Neurosci.* 16:3601–3619.

Bray, D. 1984. Axonal growth in response to experimentally applied mechanical tension. *Dev. Biol.* 102:379–389.

Bustamante, C., J. C. Macosko, and G. J. Wuite. 2000. Grabbing the cat by the tail: manipulating molecules one by one. *Nat. Rev. Mol. Cell Biol.* 1:130–136.

Buxbaum, R., and S. Heidemann. 1992. An absolute rate theory model for tension control of axonal elongation. *J. Theor. Biol.* 155:409–426.

Chada, S., P. Lamoureux, R. E. Buxbaum, and S. R. Heidemann. 1997. Cytomechanics of neurite outgrowth from chick brain neurons. *J. Cell Sci.* 110:1179–1186.

Choquet, D., D. P. Felsenfeld, and M. P. Sheetz. 1997. Extracellular matrix rigidity causes strengthening of integrin-cytoskeleton linkages. *Cell.* 88:39–48.

Crick, F. H. C., and A. F. W. Hughes. 1949. The physical properties of cytoplasm: a study by means of the magnetic particle method. *Exp. Cell Res.* 1:37–80.

Dai, J., and M. P. Sheetz. 1995. Mechanical properties of neuronal growth cone membranes studied by tether formation with laser optical tweezers. *Biophys. J.* 68:988–996.

Dennerll, T. J., P. Lamoureux, R. E. Buxbaum, and S. R. Heidemann. 1989. The cytomechanics of axonal elongation and retraction. *J. Cell Biol.* 109:3073–3083.

Dent, E. W., J. L. Callaway, G. Szebenyi, P. W. Baas, and K. Kalil. 1999. Reorganization and movement of microtubules in axonal growth cones and developing interstitial branches. *J. Neurosci.* 19:8894–8908.

Dent, E. W., and K. Kalil. 2001. Axon branching requires interactions between dynamic microtubules and actin filaments. *J. Neurosci.* 21: 9757–9769.

Gallo, G., and P. C. Letourneau. 1998. Localized sources of neurotrophins initiate axon collateral sprouting. *J. Neurosci.* 18:5403–5414.

Gallo, G., and P. C. Letourneau. 1999. Different contributions of microtubule dynamics and transport to the growth of axons and collateral sprouts. *J. Neurosci.* 19:3860–3873.

Glogauer, M., P. Arora, D. Chou, P. A. Janmey, G. P. Downey, and C. A. McCulloch. 1998. The role of actin-binding protein 280 in integrin-dependent mechanoprotection. *J. Biol. Chem.* 273:1689–1698.

Glogauer, M., P. Arora, G. Yao, I. Sokholov, J. Ferrier, and C. A. McCulloch. 1997. Calcium ions and tyrosine phosphorylation interact coordinately with actin to regulate cytoprotective responses to stretching. *J. Cell Sci.* 110:11–21.

Harrison, R. G. 1935. On the origin and development of the nervous system studied by the methods of experimental embryology. *Proc. R. Soc. Lond. B Biol. Sci.* 118:155–196.

Heidemann, S. R., and R. E. Buxbaum. 1990. Tension as a regulator and integrator of axonal growth. *Cell Motil. Cytoskeleton.* 17:6–10.

Heinrich, V., and R. E. Waugh. 1996. A piconewton force transducer and its application to measurement of the bending stiffness of phospholipid membranes. *Ann. Biomed. Eng.* 24:595–605.

Hochmuth, R. M., J.-Y. Shao, J. Dai, and M. P. Sheetz. 1996. Deformation and flow of membrane into tethers extracted from neuronal growth cones. *Biophys. J.* 70:358–369.

Huang, H., C. Y. Dong, H.-S. Kwon, J. D. Sutin, R. D. Kamm, and P. T. C. So. 2002. Three-dimensional cellular deformation analysis with a two-photon magnetic manipulator workstation. *Biophys. J.* 82:2211–2223.

Huang, H., T. Ragan, R. T. Lee, and P. T. So. 2001. Cellular deformation studies with a magnetic tweezer and particle tracking. *Ann. Biomed. Eng.* 29:S-22.

Katz, M. J., E. B. George, and L. J. Gilbert. 1984. Axonal elongation as a stochastic walk. *Cell Motil.* 4:351–370.

Kaverina, I., O. Krylyshkina, K. Beningo, K. Anderson, Y.-L. Wang, and J. V. Small. 2002. Tensile stress stimulates microtubule outgrowth in living cells. *J. Cell Sci.* 115:2283–2291.

Kitamura, K., M. Tokunaga, A. H. Iwane, and T. Yanagida. 1999. A single myosin head moves along an actin filament with regular steps of 5.3 nanometres. *Nature.* 397:129–134.

Ko, K. S., and C. A. McCulloch. 2000. Partners in protection: interdependence of cytoskeleton and plasma membrane. *J. Membr. Biol.* 174:85–95.

Lamoureux, P., R. E. Buxbaum, and S. R. Heidemann. 1989. Direct evidence that growth cones pull. *Nature.* 340:159–162.

Odde, D. J., and H. M. Buettner. 1995. Time series characterization of simulated microtubule dynamics in the nerve growth cone. *Ann. Biomed. Eng.* 23:268–286.

Odde, D. J., E. M. Tanaka, S. S. Hawkins, and H. M. Buettner. 1996. Stochastic dynamics of the nerve growth cone and its microtubules during neurite outgrowth. *Biotechnol. Bioeng.* 50:452–461.

Pettmann, B., J. C. Louis, and M. Sensenbrenner. 1979. Morphological and biochemical maturation of neurones cultured in the absence of glial cells. *Nature.* 281:378–380.

Riveline, D., E. Zamir, N. Q. Balaban, U. S. Schwarz, T. Ishizaki, S. Narumiya, Z. Kam, B. Geiger, and A. D. Bershadsky. 2001. Focal contacts as mechanosensors: externally applied mechanical force induces growth of focal contacts by an mDia1-dependent and ROCK-independent mechanism. *J. Cell Biol.* 153:1175–1185.

Schmidt, F. G., F. Ziemann, and E. Sackmann. 1996. Shear field mapping in actin networks by using magnetic tweezers. *Eur. Biophys. J.* 24:348–353.

Sensenbrenner, M., K. Maderspach, L. Latzkovits, and G. G. Jaros. 1978. Neuronal cells from chick embryo cerebral hemispheres cultivated on polylysine-coated surfaces. *Dev. Neurosci.* 1:90–101.

Smith, C. L. 1994. Cytoskeletal movements and substrate interactions during initiation of neurite outgrowth by sympathetic neurons *in vitro*. *J. Neurosci.* 14:384–398.

Smith, D. H., J. A. Wolf, T. A. Lusardi, V. M.-Y. Lee, and D. F. Meaney. 1999. High tolerance and delayed elastic response of cultured axons to dynamic stretch injury. *J. Neurosci.* 19:4263–4269.

Smith, D. H., J. A. Wolf, and D. F. Meaney. 2001. A new strategy to produce sustained growth of central nervous system axons: continuous mechanical tension. *Tissue Eng.* 7:131–139.

Suter, D. M., and P. Forscher. 1998. An emerging link between cytoskeletal dynamics and cell adhesion molecules in growth cone guidance. *Curr. Opin. Neurobiol.* 8:106–116.

Tokioka, R., A. Matsuo, K. Kiyosue, M. Kasai, and T. Taguchi. 1993. Synapse formation in dissociated cell cultures of embryonic chick cerebral neurons. *Dev. Brain Res.* 74:146–150.

Van Essen, D. C. 1997. A tension-based theory of morphogenesis and compact wiring in the central nervous system. *Nature.* 385:313–318.

Waterman-Storer, C. M., and E. D. Salmon. 1997. Actomyosin-based retrograde flow of microtubules in the lamella of migrating epithelial cells influences microtubule dynamic instability and turnover and is associated with microtubule breakage and treadmilling. *J. Cell Biol.* 139:417–434.

Weiss, P. 1941. Nerve patterns. The mechanics of nerve growth. *Growth.* 5:163–203.

Wittmann, T., and C. M. Waterman-Storer. 2001. Cell motility: can Rho GTPases and microtubules point the way? *J. Cell Sci.* 114:3795–3803.

Zheng, J., R. E. Buxbaum, and S. R. Heidemann. 1993. Investigation of microtubule assembly and organization accompanying tension-induced neurite initiation. *J. Cell Sci.* 104:1239–1250.

Zheng, J., P. Lamoureux, V. Santiago, T. Dennerll, R. E. Buxbaum, and S. R. Heidemann. 1991. Tensile regulation of axonal elongation and initiation. *J. Neurosci.* 11:1117–1125.

Zhou, F.-Q., C. M. Waterman-Storer, and C. S. Cohan. 2002. Focal loss of actin bundles causes microtubule redistribution and growth cone turning. *J. Cell Biol.* 157:839–849.